Biophysical Chemistry 144 (2009) 108–118

Contents lists available at ScienceDirect

Biophysical Chemistry

journal homepage: http://www.elsevier.com/locate/biophyschem

Conformational stabilities of guinea pig OCP1 and OCP2

Anmin Tan, Michael T. Henzl *

Department of Biochemistry, University of Missouri, Columbia, MO 65211, United States

ARTICLE INFO

Article history:
Received 22 May 2009
Received in revised form 8 July 2009
Accepted 9 July 2009
Available online 18 July 2009

Keywords:
Ubiquitin ligase
SCF complex
F-box protein
Organ of Corti
Protein stability
Calorimetry

ABSTRACT

OCP1 and OCP2, the most abundant proteins in the cochlea, are evidently subunits of an SCF E3 ubiquitin ligase. Although transcribed from a distinct gene, OCP2 is identical to Skp1. OCP1 is equivalent to the F-box protein known as Fbs1, Fbx2, or NFB42 — previously shown to bind N-glycosylated proteins and believed to function in the retrieval and recycling of misfolded proteins. The high concentrations of OCP1 and OCP2 in the cochlea suggest that the OCP1–OCP2 heterodimer may serve an additional function independent of its role in a canonical SCF complex. At 25 °C, urea-induced denaturation of OCP1 is slow, but reversible. The data suggest that the protein possesses one or more disordered regions, a conclusion supported by analysis of the far-UV circular dichroism spectrum and the appearance of the ^{1}H, ^{15}N-HSQC spectrum. Thermal denaturation of OCP1 is irreversible, evidently due to formation of high molecular weight aggregates. Analysis with a kinetic model yields an estimate for the activation energy for unfolding of 49 kcal/mol. Urea denaturation data for OCP2 returns ΔG_o and m values of 6.2 kcal/mol and 1.5 kcal mol^{-1} M^{-1}, respectively. In contrast to OCP1, thermal denaturation of OCP2 is reversible. In phosphate-buffered saline, at pH 7.40, the protein exhibits a $\Delta H_{vH}/\Delta H_{cal}$ ratio of 1.69, suggesting that denaturation proceeds largely from the native dimer directly to the unfolded state. OCP1 and OCP2 associate tightly at room temperature. However, DSC data for the complex suggest that they denature independently, consistent with the highly exothermic enthalpy of complex formation reported previously.

1. Introduction

The mammalian auditory system has three major components — the inner- and outer hair cells (IHC and OHC, respectively), the supporting cell population, and the stria vascularis (SV) [1]. The hair cells and supporting cells constitute the auditory organ *per se*, the organ of Corti (OC). The solution bathing the hair cells, endolymph, is distinguished by a high K^+ content (150 mM) and strongly positive electrochemical potential (+100 mV). As a consequence, the hair cells experience a continuous K^+ flux, often called the "standing K^+ current." The SV is responsible for the secretion of K^+ into the endolymph.

Auditory perception begins with modulation of the standing K^+ current. Vibration of the basilar membrane supporting the OC, in response to acoustic input, causes mechanical deflection of stereocilia lining the apical IHC and OHC surfaces. This deflection opens transduction channels, thereby increasing the K^+ flux. In the IHC, the ensuing depolarization stimulates release of neurotransmitters and subsequent excitation of the auditory neurons. In the OHC, depolarization stimulates "electromotility" — audiofrequency cycles of axial contraction and elongation that amplify the original acoustic signal.

The post-mitotic hair cells, which must survive for decades in humans, face a formidable challenge in the OC. The absence of vasculature complicates nutrient transport and waste metabolite clearance. Moreover, the endolymphatic potential, besides driving the standing K^+ current, also promotes the continuous influx of Ca^{2+} through the relatively non-selective transduction channels. Responsibility for maintaining homeostasis and maximizing sensory cell survival rests primarily with the supporting cell population, also called the epithelial support complex (ESC).

The ESC includes twelve distinct cell types [2]. Despite their morphological heterogeneity, they are united by an extensive network of gap-junctions [3,4]. In addition to cell-type specific functions, the ESC functions collectively to perform transcellular transport of low-molecular weight species. The importance of this activity is illustrated by the association between non-syndromic hereditary deafness disorders and mutations in connexin 26 (Cx26) — a major gap-junction protein expressed in the ESC [5,6]. The available data suggest that Cx26 lesions permit accumulation of toxic levels of glutamate in the vicinity of the IHC [7].

OCP1 and OCP2 were discovered during an electrophoretic survey of OC proteins [8]. They are the two most abundant proteins in the OC, accounting for approximately 10% of the total protein. Their

* Corresponding author. Department of Biochemistry, 117 Schweitzer Hall, University of Missouri, Columbia, MO 65211, United States. Tel.: +1 573 882 7485; fax: +1 573 884 4812.
E-mail address: henzlm@missouri.edu (M.T. Henzl).

0301-4622/$ – see front matter © 2009 Elsevier B.V. All rights reserved.
doi:10.1016/j.bpc.2009.07.003

distribution coincides identically with the gap-junction system uniting the ESC [9], prompting speculation that they may be involved in the regulation of gap-junction activity. In our hands, an anti-OCP1 antibody co-precipitated connexin 26 from soluble OC extracts [10]. Likewise, an anti-Cx26 antibody preparation co-precipitated OCP2. Consistent with these findings, implying that OCP1 associates noncovalently with Cx26, we found that immobilized OCP1 will pull down radiolabeled Cx26 produced by *in vitro* transcription/translation. Significantly, however, Nelson et al. did not detect an interaction between Fbx2, the OCP1 ortholog in mouse, and Cx26, in either mouse cochlea or transfected cells [11]. Thus, the physiological relevance of our observations is questionable.

Sequence analysis suggests that OCP1 and OCP2 are components of an SCF E3 ubiquitin ligase, a multi-subunit complex that directs ubiquitination of specific proteins [12,13]. SCF is an acronym for *S*kp1, *c*ullin, and *F*-box protein — the first three subunits of the complex to be characterized. SCF complexes bind select target proteins and position them for ubiquitination by an E2 ubiquitin-conjugating enzyme. The F-box protein, which binds to Skp1 through a characteristic F-box motif, determines target-protein specificity [14,15].

The sequence of OCP2 (Fig. 1A) is identical to Skp1, although it is transcribed from a distinct gene [16]. OCP1 is an F-box protein, evidently the same gene product variously referred to as Fbs1, Fbg1, NFB42, or Fbx2 [17,18]. OCP1/Fbs1 and OCP2/Skp1 associate avidly [10,19]. A ribbon diagram of the complex formed between Skp1 (magenta) and Fbs1 (cyan) is displayed in Fig. 1C. The guinea pig OCP1 sequence (Fig. 1B) exhibits 83% identity to murine Fbs1. The belief that OCP1 and OCP2 play a vital role in the auditory system is supported by the recent demonstration by Nelson et al. that ablation of the mouse Fbx2 gene markedly accelerates age-related hearing loss [11]. Fbs1 has been shown to bind glycosylated proteins, where the polysaccharide moiety has the structure $Man_nGlcNac_2$ ($n \geq 2$) [20]. The SCF^{Fbs1} ligase is believed to mediate the proteolytic degradation of misfolded proteins recovered from the endoplasmic reticulum [17]. Thus, Nelson et al. have suggested that OCP1/Fbs1 and OCP2/Skp1 are involved in glycoprotein quality control in the OC.

We have commented previously on the decided excess of OCP1 and OCP2 relative to the other two canonical SCF subunits, cullin and Rbx1 [21,21]. An accumulating body of circumstantial evidence suggests that OCP2/Skp1 and OCP1/Fbs1 also form an atypical heterodimer in the cochlea. There is precedent for this behavior. Although RCY1, an F-box protein in yeast, binds Skp1 and participates in the recycling of internalized proteins, it evidently does not form an SCF complex [22]. Yoshida et al. have suggested, on the basis of cell-based studies, that the OCP1/Fbx2-OCP2/Skp1 heterodimer may serve to prevent glycoprotein aggregation [23]. This circumstance is compelling motivation for detailed biophysical characterization of the two proteins. As part of an ongoing effort to characterize the physical properties of these interesting proteins, we present an evaluation of their conformational stabilities.

2. Materials and methods

2.1. Reagents and chemicals

NaCl, sodium phosphate (monobasic, anhydrous), lysozyme, Spectrapor dialysis tubing (MWCO 12,000–14,000), N,N′-methylene-bis-acrylamide, and acrylamide were purchased from Fisher Scientific Co. LB agar, LB broth, ampicillin, kanamycin, and chloramphenicol were obtained from Research Products International. IPTG and DTT were purchased from Gold Biotechnology. DEAE-Sepharose, Sephadex G-75, Sephacryl S-100-HR, tris(hydroxypropyl) phosphine (THP), and ultra-pure urea (Fluka) were obtained from Sigma-Aldrich Co. Ni-NTA His-Bind resin was obtained from QIAGEN. BenchMark Pre-Stained

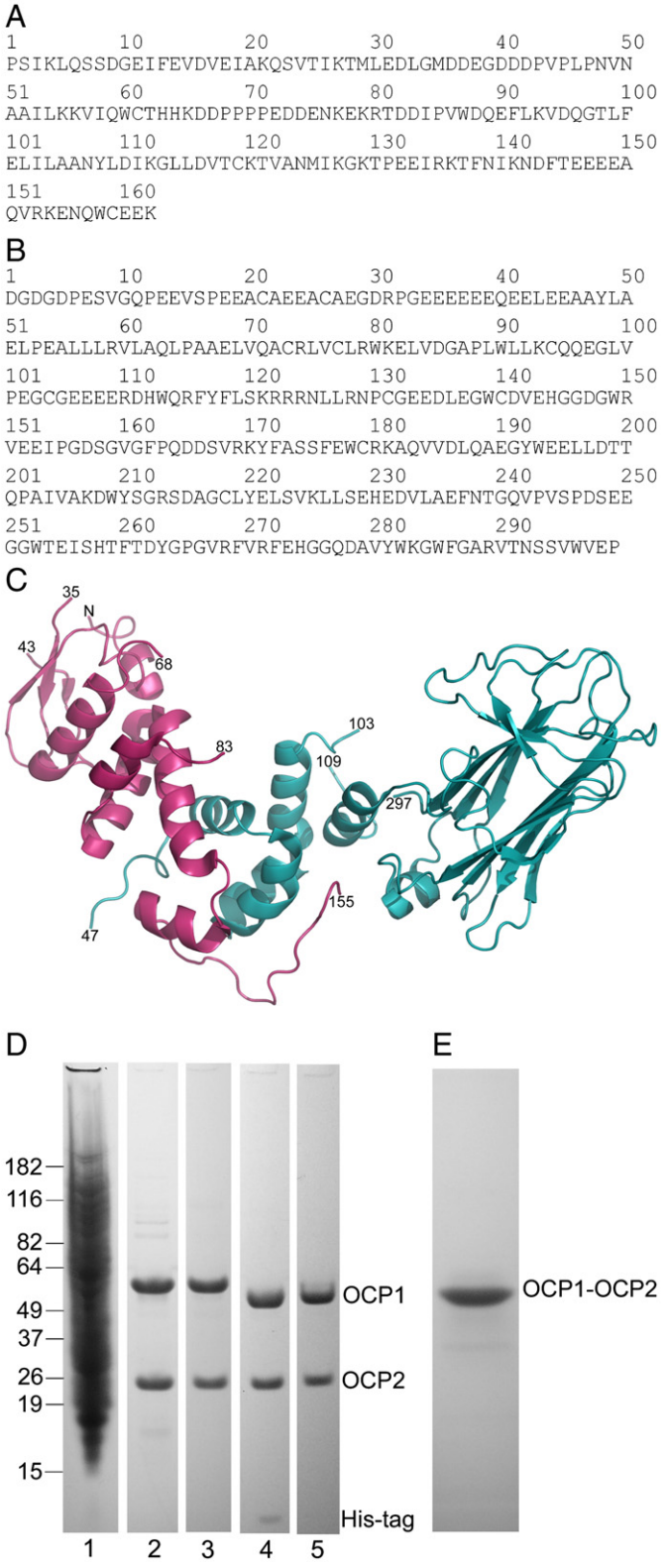

Fig. 1. (A) Amino acid sequence of guinea pig OCP2. (B) Amino acid sequence of guinea pig OCP1. (C) Ribbon diagram of the complex formed between human Skp1 and murine Fbs1. Figure prepared in PyMol [36], using the atomic coordinates from PDB 2E31. Note that residues 36–42, 69–82, and 156–162 are not observed in the structure of Skp1. Similarly, residues 1–46 and 104–108 are not observed in the Fbs1 structure. (D) Isolation of the OCP1–OCP2 complex. Samples collected at each stage of purification were subjected to SDS-PAGE through a 4–12% NuPage Bis–Tris gel and stained with Coomassie Blue G250. Lane 1, clarified bacterial lysate; lane 2, after DEAE-Sepharose chromatography; lane 3, following elution from Ni-NTA agarose; lane 4, immediately after treatment with thrombin; lane 5, after Sephacryl S100 chromatography. The mobilities of pre-stained molecular weight markers are indicated at left. (E) An aliquot of the purified OCP1–OCP2 complex was subjected to electrophoresis through a 10% polyacrylamide gel under nondenaturating conditions and visualized with Coomassie Blue G250.

Protein Ladder and 4–12% NuPage Bis–Tris gels were purchased from Invitrogen.

2.2. Protein expression and purification

The guinea pig OCP2 coding sequence was cloned into pTriEx-1.1 (Novagen), between the Nco I and BamH I sites. The coding sequence of guinea pig OCP1 [9] was cloned between the Nco I and BamH I sites of pET28a (Novagen), immediately downstream from the N-terminal hexa-histidine tag and thrombin cleavage site. The protocols used to isolate the individual proteins are described elsewhere [19]. Native guinea pig OCP1, containing 299 residues, has a sequence-derived molecular weight of 33,682. After removal of the His tag, the recombinant protein expressed by the OCP1–pET28 construct harbors a four-residue N-terminal extension, Gly-Ser-His-Met, which raises the molecular weight to 34,094. CDPro [24] was used to estimate the secondary structure content of OCP1 in PBS at pH 7.4.

The OCP1–OCP2 complex was isolated from *E. coli* BL21(DE3) Rosetta 2 cells (Novagen) harboring both OCP1–pET28 and OCP2–pTriEx1.1. Because the two vectors contain distinct antibiotic-resistance markers, it is possible to maintain selection for both, even though they have the same origin of replication. Six 1-L cultures of the bacteria — in LB broth supplemented with ampicillin (100 μg/mL), kanamycin (50 μg/mL), and chloramphenicol (30 μg/mL) — were incubated at 37 °C. When the absorbance at 600 nm reached 0.6, IPTG was added to a final concentration of 0.25 mM, and incubation was continued for an additional 6 h. The bacteria were collected by centrifugation at 4 °C and resuspended in four volumes of 20 mM Hepes–NaOH, pH 7.4, supplemented with Complete® protease inhibitor cocktail (Roche Molecular Biochemicals).

The cells were disrupted with a French pressure cell, following treatment with lysozyme (15 min at 37 °C, 5 mg enzyme per gram of cell paste), and the clarified lysate was loaded onto DEAE-Sepharose (4 mL L^{-1} of culture). The column was then eluted with a 0–0.6 M NaCl gradient (10 column bed volumes), prepared in Hepes–NaOH, pH 7.4. Fractions containing the complex, identified by nondenaturing PAGE, were combined and loaded onto Ni-NTA agarose. After washing the column bed extensively with 0.30 M NaCl, 0.05 M NaP_i, pH 8.0, ($NaCl/NaP_i$ buffer) containing 20 mM imidazole, the OCP1–OCP2 complex was liberated with 0.25 M imidazole in $NaCl/NaP_i$ buffer.

After overnight dialysis against PBS (0.15 M NaCl, 0.01 M NaP_i, pH 7.4), the preparation was treated with thrombin (Novagen, 1 U/mg OCP1–OCP2 complex), for 4 h on ice, to release the hexa-histidine tag. After confirming that cleavage was complete, by SDS-PAGE, the thrombin was inactivated with PMSF (1 mM) and DTT (10 mM). The complex was then concentrated to 2–3 mL and subjected to gel-filtration chromatography through Sephacryl S100. Fortuitously, the culture produces an excess of OCP2, which lacks the histidine tag. Thus, the extract contains essentially no free OCP1, which would otherwise bind to the Ni-NTA matrix and complicate the isolation procedure.

The progress of the purification, as monitored by electrophoresis, is depicted in Fig. 1. Panel D presents an SDS-PAGE analysis of samples obtained after lysis (lane 1), DEAE-Sepharose Chromatography (lane 2), Ni-NTA agarose chromatography (lane 3), thrombin treatment (lane 4), and Sephacryl S100 chromatography (lane 5). Panel E depicts the behavior of the purified complex when subjected to PAGE under nondenaturing conditions. The avidity of the complex is sufficiently high that the complex remains intact during the one-hour nondenaturing separation.

Concentrations of OCP2 and OCP1 were estimated spectrophotometrically — employing extinction coefficients at 280 nm of 19,400 and 81,000 M^{-1} cm^{-1}, respectively, determined by parallel absorbance and interference measurements in the analytical ultracentrifuge. The extinction coefficient of OCP1–OCP2 was assumed to be 100,400 M^{-1} cm^{-1}, the sum of the values for the individual proteins.

2.3. Urea denaturation studies

OCP2. Denaturation of OCP2 by urea was monitored by CD at 222 nm, employing an Aviv 62DS spectrometer. Titrations were performed in PBS/THP — i.e., phosphate-buffered saline containing 1.0 mM tris (hydroxypropyl)phosphine — using an auto-titrator (Hamilton Microlab 500) interfaced with the spectrometer. The experiments were conducted in 10 mm cuvettes, in a constant volume of 2.0 mL. Following each addition, the sample was stirred for 60 s prior to observation. At each point, the signal was averaged for 30 s. Reversibility was tested by comparing the signals produced by mixing 1) equal volumes of 8.0 M urea and native protein solution and 2) equal volumes of buffer and denatured (8.0 M urea) protein.

The ellipticity data for denaturation of OCP2 alone, corrected for dilution, were treated with Eqs. (1) and (2), a modification of the two-state unfolding model proposed by Santoro and Bolen [25]:

$$P = 1 + 2K_a[OCP2] + K_u \tag{1}$$

$$y = \frac{(y_n + m_n[urea])(1 + 2K_a[OCP2])}{P} + \frac{(y_n + m_n[urea])K_u}{P}. \tag{2}$$

In Eq. (1), P represents the partition function for OCP2, with contributions from the monomeric, dimeric, and unfolded protein. K_a is the association constant for dimer formation. K_u is the equilibrium constant for unfolding, given by

$$K_u = \exp[-\Delta G_u / RT] = \exp[-(\Delta G_o - m[urea]) / RT] \tag{3}$$

where ΔG_o is the free energy change for unfolding in the absence of urea; m describes the sensitivity of the conformational free energy to urea concentration; [*urea*] is the total urea concentration; R is the gas constant; and T is the absolute temperature. The term [*OCP2*] in Eq. (1) represents the free monomer concentration, equal to

$$[OCP2] = \left(\sqrt{1 + 8K_a[OCP2]_{tot}} - 1\right) / 4K_a \tag{4}$$

where $[OCP2]_{tot}$ is the total concentration of OCP2 concentration, expressed as monomer.

In Eq. (2), the first term represents the ellipticity contributions from the monomeric and dimeric forms of the native protein. y_n and m_n denote the slope and intercept of the pre-transition baseline. The second term represents the denatured state contribution to the ellipticity signal, with y_u and m_u specifying the slope and intercept of the post-transition baseline.

Because OCP1 unfolds very slowly in urea (vide infra), when one monitors the urea-induced denaturation of the OCP1–OCP2 complex by CD, the short-term change in ellipticity reflects exclusively the unfolding of OCP2. The model used to treat that phenomenon is similar to that used to treat unfolding of the OCP2 homodimer:

$$P = 1 + K_a[OCP1] + K_u \tag{5}$$

$$y = \frac{(y_n + m_n[urea])(1 + K_a[OCP1])}{P} + \frac{(y_n + m_n[urea])K_u}{P} \tag{6}$$

In Eqs. (5) and (6), K_a is the equilibrium constant for formation of the OCP1–OCP2 heterodimer; [*OCP1*] represents the free OCP1 concentration; and the other terms were defined above.

OCP1. Slow unfolding kinetics precluded use of the auto-titrator for studying the denaturation of OCP1 by urea. Instead, individual samples of OCP1 were prepared in PBS/THP for each urea concentration of interest. Following a 16 h equilibration period, the far-UV circular dichroism spectrum of each sample was collected.

The concentration of OCP1 in the samples was sufficiently low that the self-associative tendency could be neglected. Thus, after

subtracting out the buffer contribution, the ellipticity values at 221 nm were fit to a standard two-state unfolding model [25].

$$y = \frac{(y_n + m_n[urea]) + (y_u + m_u[urea]) * \exp(-(\Delta G_o - m[urea])/RT)}{1 + \exp(-(\Delta G_o - m[urea])/RT)} \quad (7)$$

where all of the terms were defined above.

The 10.0 M urea titrant used in the OCP1 and OCP2 unfolding experiments was prepared by transferring 60.06 g urea to a 100 mL volumetric flask, then adding 10.0 mL of 10× PBS and sufficient water to achieve dissolution of the urea. Following dilution to 100 mL, the pH was adjusted to pH 7.4 with 6 M HCl. The concentration determined by refractometry agreed with the calculated value to within 0.05 M. The solution was divided into aliquots and stored at −20 °C. Aliquots were thawed once, then discarded.

Differential scanning calorimetry (DSC) was performed in a modified Nano-DSC (Calorimetry Sciences Corporation) equipped with cylindrical hastalloy cells, having a nominal volume of 0.32 mL. Samples were dialyzed to equilibrium against PBS/THP, which then served as the reference buffer. Sample and reference solutions were briefly placed under vacuum prior to loading, to reduce the concentrations of dissolved gases. Temperature calibration was verified with solutions of dimyristoyl-, dipalmitoyl-, and distearoylphosphatidyl choline. The accuracy of the differential power measurements was verified with internally generated electrical calibration pulses.

OCP1. The kinetically controlled denaturation of OCP1 was modeled using a standard Arrhenius treatment of the direct conversion of the native state to an irreversibly denatured product [26,27]. Initially, a buffer baseline was subtracted from the protein denaturation data. The pre- and post-transition baselines were then fit to a fourth-order polynomial, which was then subtracted from the protein data to give an apparent excess heat capacity function, $C_{p,ap}$. The latter is given by

$$C_{p,ap} = \left(-\frac{dP_n}{dT}\right) * \Delta H_{ap} \quad (8)$$

where ΔH_{ap} is the apparent total enthalpy associated with the process and $-dP_n/dT$ describes the temperature-dependent depopulation of the native state. Although ΔH_{ap} has no direct thermodynamic significance, it reflects the total enthalpy change that accompanies the conversion. $-dP_n/dT$ is related to the time-dependent rate of depopulation of the native state, $-dP_n/dt$, through the calorimeter scan rate, *sr*

$$-\frac{dP_n}{dT} = \left(\frac{1}{sr}\right)\left(-\frac{dP_n}{dt}\right) \quad (9)$$

For a first-order reaction,

$$-\frac{dP_n}{dt} = kP_n = \left[A\exp\left(\frac{-E_a}{RT}\right)\right]P_n \quad (10)$$

where k is the first-order rate constant, A is the pre-exponential term, E_a is the activation energy for the process. Substituting this expression into Eq. (8) yields

$$-\frac{dP_n}{dT} = \left(\frac{A}{sr}\right)\exp\left(\frac{-E_a}{RT}\right)P_n(T) \quad (11)$$

The values of $P_n(T)$ are obtained by integrating eq. (11).

$$P_n(T) = \exp\left(\frac{1}{sr} \cdot \int_{T_o}^{T} A \cdot \exp\left(\frac{-E_a}{RT}\right)dT\right) \quad (12)$$

where T_o is some temperature at which no unfolding has occurred. Least-squares minimization was performed with a Fortran routine written in-house. Parameter uncertainties were determined by Monte Carlo simulation.

An initial estimate of E_a was obtained from an Arrhenius plot. Estimates of k were obtained using the equation developed by Sanchez-Ruiz [26]:

$$k = \frac{sr * C_{p,xs}}{\Delta H_{ap} - Q(T)} \quad (13)$$

where $C_{p,xs}$ is the apparent molar heat capacity, ΔH_{ap} (the apparent enthalpy) is the total area under the curve, and $Q(T)$ is the area of the curve between T_o and T. The values so obtained were used to construct a plot of $\ln k$ vs $1/T$. The slope of the linear region of that plot equals $-E_a/R$.

OCP2. A baseline, obtained with sample- and reference cells filled with buffer, was subtracted from the protein data prior to analysis. The resulting heat capacity data, c_p, having units of mcal K^{-1}, were analyzed with the following two-state model [28]:

$$c_p = \left(\frac{10^3 mc * V}{MW}\right)\left(\left[\Delta H_c(T_m) + \beta\Delta C_p(T - T_m)\right] \times \left[\frac{\Delta H_{vH}(T_m) + \Delta C_p(T - T_m)}{RT^2}\right]\left(\frac{K(T)}{(1 + K(T))^2}\right) + a + \left(\frac{1}{1 + K(T)}\right)(b*(T - T_m)) + \left(\frac{K(T)}{1 + K(T)}\right)\left(\Delta C_p + d*(T - T_m)\right)\right) \quad (14)$$

In this equation, *mc* is the protein concentration in g/L, V is the sample cell volume in L, *MW* is the protein molecular weight, $\boldsymbol{\beta}$ is the ratio of calorimetric and van't Hoff enthalpies (ΔH_c and ΔH_{vH}), ΔC_p is the heat capacity change upon denaturation (assumed to be temperature-independent), T is the absolute temperature, T_m is the transition midpoint, and R is the gas constant. $K(T)$ is the temperature-dependent equilibrium constant

$$K(T) = \exp(-\Delta G(T)/RT) \quad (15)$$

where $\Delta G(T)$ is given by the Gibbs–Helmholtz equation:

$$\Delta G(T) = \Delta H\left(\frac{T_m - T}{T_m}\right) + \Delta C_p\left[(T - T_m) - T\ln\frac{T}{T_m}\right]. \quad (16)$$

Weighted least-squares analysis was performed with Origin v.7.5, assuming a uniform standard deviation of 0.003 mcal/K. To improve the estimates for ΔH_{cal} and ΔC_p, data collected at two protein concentrations were modeled simultaneously. T_m, ΔH_{cal}, ΔH_{vH} and ΔC_p were treated as global variables and allowed to float during the fitting procedure. The baseline parameters (a, b, d) were local parameters, unique to each scan, and were likewise allowed to vary. The protein concentrations were fixed at the values determined by UV absorbance.

To further improve the estimation of ΔC_p in the analysis of OCP2, urea denaturation data were subjected to nonlinear least-squares minimization along with the DSC data. The equation used to treat the chemical denaturation data was identical to Eq. (7), except that ΔG_o was not explicitly used as a fitting parameter. Rather, its value was calculated from the Gibbs–Helmholtz equation:

$$\Delta G_o = \Delta H_{vH}\left(\frac{T_m - T_{urea}}{T_m}\right) + \Delta C_p[(T_{urea} - T_m) - T_{urea}\ln(T_{urea}/T_m)] \quad (17)$$

Thus, the optimal values of T_m, ΔH_{vH}, and ΔC_p were selected to accommodate both types of data. Inclusion of the urea denaturation data had little impact on the T_m and ΔH_{vH}. However, the value of ΔC_p, poorly determined when the DSC data were analyzed in isolation, was well-defined with inclusion of the chemical unfolding data.

Sedimentation velocity data were collected on heat-treated OCP1, using a Beckman Optima XL-I centrifuge and dual-sector charcoal-Epon centerpieces. The rotor was allowed to equilibrate at the desired temperature for 2 h prior to beginning the run. Data collection was initiated immediately following rotor acceleration and was continued until 150 radial distributions had been acquired. The resulting data were analyzed with Sedfit [29], employing the continuous $c(s)$ distribution model. The partial specific volume of OCP1 was estimated at 0.71 cm^3/g, based on its amino acid compositions. Solvent densities were measured with an Anton-Paar DMA 5000 densimeter.

NMR spectroscopy. ^{15}N-labeled preparations of OCP1 and OCP1–OCP2 were isolated, as described above, from bacteria cultured on ^{15}N-Spectra 9 medium (Cambridge Isotope Laboratories, Inc). ^1H,^{15}N-HSQC spectra were collected on 0.3 mM samples of the proteins at 25 °C. The samples also contained 0.15 M NaCl, 0.01 M NaPi, pH 6.0, 0.002 M THP, 10% D_2O. Data acquisition was performed with a Varian Inova 600 MHz spectrometer, equipped with a triple-resonance cryoprobe. Data were acquired with the Varian BioPack N15-HSQC pulse sequence, employing the TROSY option; processed with NMRPipe [30]; and visualized with Sparky [31]. The ^1H chemical shift was referenced relative to sodium 2,2-dimethyl-2-silapentane-5-sulfonate (DSS); the ^{15}N shift was referenced indirectly.

3. Results

3.1. Stability of OCP1/Fbs1

3.1.1. Urea denaturation

The far-UV circular dichroism (CD) spectrum of OCP1 is displayed in Fig. 2A. Analysis of those data with CDPro indicated that, at pH 7.4 in PBS, the secondary structure of the protein includes an estimated 18% helix, 28% strand, and 22% turn. Thus, roughly 30% of the protein does not adopt a regular structure.

OCP1 exhibits slow unfolding kinetics at 25 °C. Denaturation in 8 M urea, monitored by CD at 221 nm, yields the relaxation curve displayed in Fig. 2B. The solid line represents the best least-squares fit to a dual-exponential model. The more rapid phase, accounting for 19% of the total change in ellipticity, occurs with a rate constant of 7.4 $(0.4)\times10^{-4}$ s^{-1}. The slower phase is characterized by a rate constant of 8.0 $(0.1)\times10^{-5}$ s^{-1} (Table 1). Refolding occurs too rapidly to monitor by manual mixing methods. Urea-induced denaturation is evidently reversible. When OCP1 is allowed to denature in the presence of 6 M urea for 16 h at 25 °C and then diluted to 0.75 M, the spectrum is indistinguishable from that of native protein incubated for 16 h in 0.75 M urea (Fig. 2C).

The slow unfolding behavior prevented acquisition of a complete denaturation profile on a single sample. Thus, individual samples of OCP1/Fbs1 (5 μM) were prepared at urea concentrations between 0 and 8 M. After 16 h at 25 °C, they were examined by CD. Data from four separate analyses are displayed in Fig. 3. Global analysis of the four data sets, employing a two-state model for denaturation, returned a ΔG_o of 2.64 ± 0.36 kcal/mol and an m value of 0.79 ± 0.09 kcal $mol^{-1}M^{-1}$.

3.1.2. Differential scanning calorimetry

Following dialysis to equilibrium against PBS/THP, samples of OCP1/Fbs1 (140 μM) were analyzed by DSC. As shown in Fig. 4A, the transition is asymmetric, and the apparent T_m is visibly scan rate dependent — ranging from 54.8 °C at 30° h^{-1}, to 57.0 °C at 60° h^{-1} to 58.3 °C at 120° h^{-1}. Moreover, no endotherm is observed upon rescan. Evidently, thermal denaturation of OCP1 is not thermodynamically reversible. Rather, the process is kinetically controlled, due to coupling of the unfolding reaction to some subsequent irreversible event. It should be noted that reversible behavior is not achieved simply by lowering the concentration (vide infra).

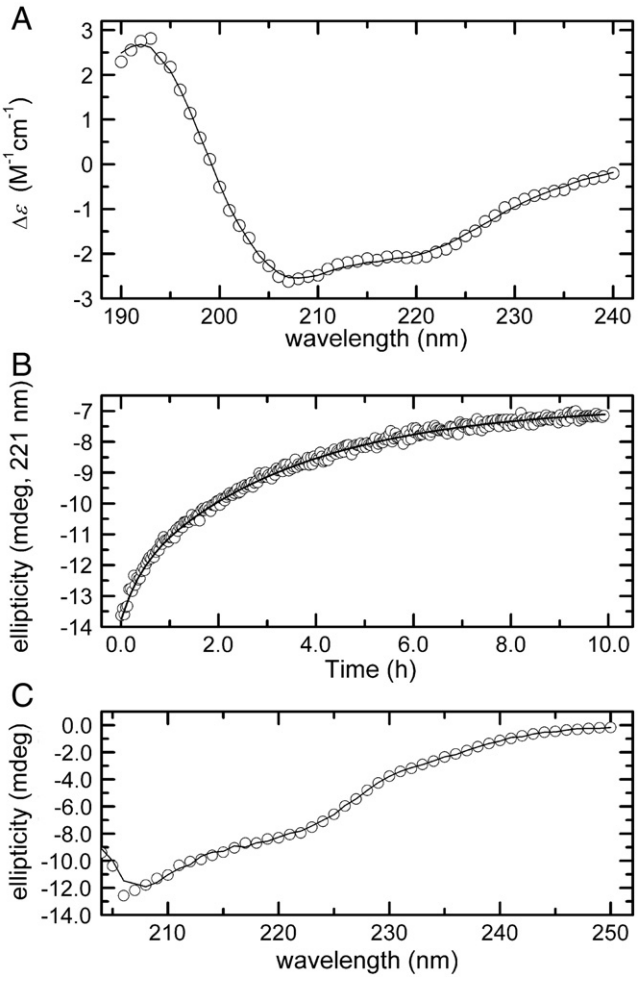

Fig. 2. Kinetics and reversibility of OCP1 chemical denaturation. (A) Analysis of OCP1 secondary structure by far-UV circular dichroism. The solid line represents the best fit to the data by the CONTIN module of CDPro. (B) Time course of denaturation of OCP1 in 8 M urea at 25 °C. Solid line represents the best fit to a dual-exponential function. (C) Reversibility of denaturation. After incubating a 40 μM sample of OCP1 for 16 h at 25 °C in PBS containing 6 M urea, the protein was diluted to 5.0 μm with PBS. The far-UV CD spectrum of the resulting solution is displayed as a solid line, along with the spectrum of 5.0 μM OCP1 that had been equilibrated under identical conditions in 0.75 M urea/PBS (○).

Thus, the DSC data were analyzed with a kinetic model. An initial estimate of the activation energy, E_a, was obtained from Arrhenius analysis, as described by Sanchez-Ruiz et al. [26]. The rate constant for denaturation, k, was estimated as a function of temperature in the vicinity of the transition, using Eq. (13), and ln$k$ was then plotted vs. $1/T$. The slope of the linear region equals $-E_a/R$. Arrhenius plots for the data from Fig. 4A are shown in Fig. 4B. Activation energies of 53.2, 51.8, and 47.5 kcal/mol, respectively, were obtained for DSC data acquired at scan rates of 30, 60, and 120° h^{-1}.

These values of E_a were then employed in least-squares analyses of the heat capacity data, using Eqs. (8)–(12), to extract estimates for the apparent enthalpy change (ΔH_{ap}) and pre-exponential factor (A) for each of the three data sets. Because global analysis of data acquired at scan rates of 0.5, 1.0, and 2.0° min^{-1} failed to yield a satisfactory fit, the data sets were modeled individually. The optimal least-squares fits, offset for clarity, are displayed in Fig. 4C.

No systematic variation was observed for either E_a or A. The former ranged from 47.7 at 2.0° min^{-1}, to 50.0 kcal/mol at 1.0° min^{-1}, to 49.3 at 0.5° min^{-1}. Similarly, the pre-exponential factor varied from 1.6×10^{31} at the highest scan rate, to 4.1×10^{32} at the intermediate scan rate, to 1.2×10^{32} at the lowest rate. The ΔH_{ap} values trend increased

Table 1
Data summary.

OCP1
Unfolding kinetics (25 °C, 8 M urea): $k_1 = 7.4 \pm 0.4 \times 10^{-4}$ s^{-1}; relative amplitude = 0.19 $k_2 = 8.0 \pm 0.1 \times 10^{-5}$ s^{-1}; relative amplitude = 0.81
Urea denaturation (25 °C): $\Delta G_o = 2.64 \pm 0.3$ kcal/mol; $m = 0.79 \pm 0.09$ kcal mol^{-1} M^{-1}
Thermal denaturation (60° h^{-1}): $T_{m,\ app} = 57$ °C; $\Delta H_{app} = 141$ kcal mol; $A = 1.2 \times 10^{32}$; and $E_a = 49.6$ kcal/mol
Sedimentation velocity: Heat treatment (5 min, 70 °C) produced additional species at 27.5 S, 31.5 S, and 34.6 6 S.
OCP2
Urea denaturation $\Delta G_o = 6.15 \pm 0.10$ kcal mol^{-1}; $m = 1.4 \pm 0.02$ kcal mol^{-1} M^{-1}
Thermal denaturation: $T_m = 6\ .4 \pm 0.1$ °C $\Delta H_{vH} = 102.2 \pm 0.3$ kcal/mol $\Delta H_{cal} = 60.4 \pm 0.3$ kcal/mol $\Delta C_p = 2.10 \pm 0.04$ kcal mol^{-1} K^{-1}
OCP1/OCP2
Urea denaturation (25 °C): $\Delta G_o = 6.34 \pm 0.10$ kcal mol^{-1}; $m = 1.55 \pm 0.08$ kcal mol^{-1} M^{-1}
Thermal denaturation (60° h^{-1}): Peaks in the excess heat capacity curve are observed at 57.4 °C and 69.4 °C.

from 126 to 141 to 151 kcal/mol with increasing scan rate (Fig. 4A, inset).

The theory of absolute reaction rates posits that reactants are in thermodynamic equilibrium with the transition state. The relevant equilibrium constant, often symbolized $K^{\neq}$, is related to the rate constant k by the expression

$$k = \frac{kT}{h} K^{\neq} \tag{18}$$

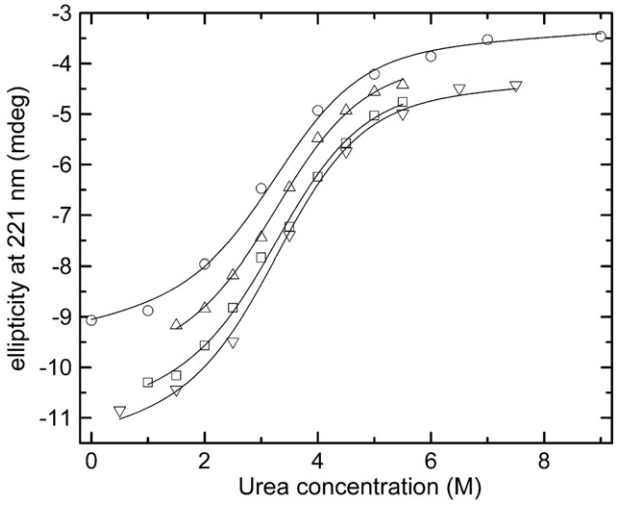

Fig. 3. Urea denaturation of OCP1. Urea (10 M in PBS) was added to aliquots of OCP1 to yield a final protein concentration of 5.0 μM and urea concentrations between 0.5 and 8.5 M. After incubation for 16 h at room temperature, the samples were analyzed by circular dichroism. The experiment was performed four times, each time employing a different set of urea concentrations. The four data sets were analyzed simultaneously, using Eq. (7), to obtain estimates of ΔG_o, the conformational stability at zero urea concentration, and m. The data and optimal least-squares fit have been offset vertically for clarity.

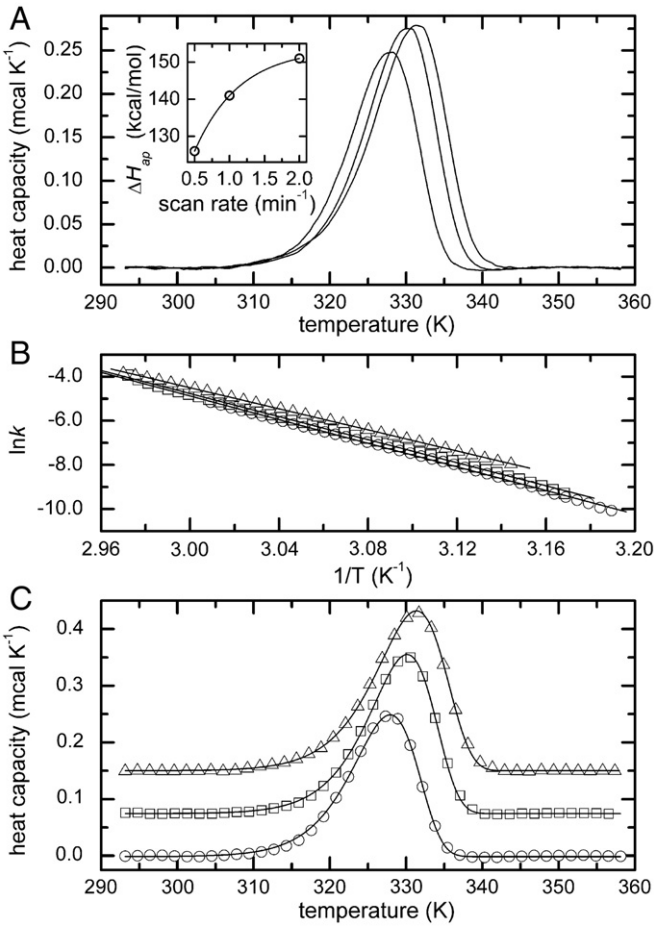

Fig. 4. (A) Thermal denaturation of OCP1 is irreversible. Samples of OCP1 (170 μM) were analyzed by DSC, employing scan rates of 0.5, 1.0, and 2.0° min^{-1}. The shift in the heat capacity maximum to higher temperature with increasing scan rate is indicative of irreversible denaturation. Inset: Apparent denaturational enthalpy as a function of scan rate. (B) The unfolding rate was estimated, as a function of temperature, by the method of Sanchez-Ruiz et al. and plotted as ln$k$ vs. $1/T$. Linear least-squares analysis was performed on subsets of the data exhibiting linear behavior. The optimal fits, indicated by the solid lines, afforded preliminary estimates for the activation energies for denaturation at each scan rate. (C) Nonlinear least-squares analysis of OCP1 thermal unfolding.

where h is Planck's constant and k is the Boltzmann constant. $K^{\neq}$ can be expressed in terms of an associated free energy change and its corresponding enthalpic and entropic components.

$$k = \frac{kT}{h}\exp\left(-\Delta G^{\neq}/RT\right) = \frac{kT}{h}\exp\left(\Delta S^{\neq}/R\right)\exp\left(-\Delta H^{\neq}/RT\right) \tag{19}$$

By comparison with Eq. (18), it is apparent that $\Delta H^{\neq}$ is identical to E_a and that the pre-exponential term A is equal to

$$A = \frac{kT}{h}\exp\left(\Delta S^{\neq}/R\right) \tag{20}$$

Substituting the pre-exponential values obtained at 2.0, 1.0, and 0.5° min^{-1} into this expression yields corresponding estimates for $\Delta S^{\neq}$ of 83.7, 90.2, and 87.7 cal deg^{-1} mol^{-1}. At 330 K, these values produce $-T\Delta S^{\neq}$ contributions of −27.6, −29.8, and −29.0 kcal/mol.

3.1.3. Sedimentation velocity analysis of heat-denatured OCP1

Aggregation is a likely cause of irreversible thermal denaturation. To determine whether OCP1 aggregates upon heating, a sample of the protein (12.3 μM) was incubated at 70 °C for 5 min, rapidly cooled to

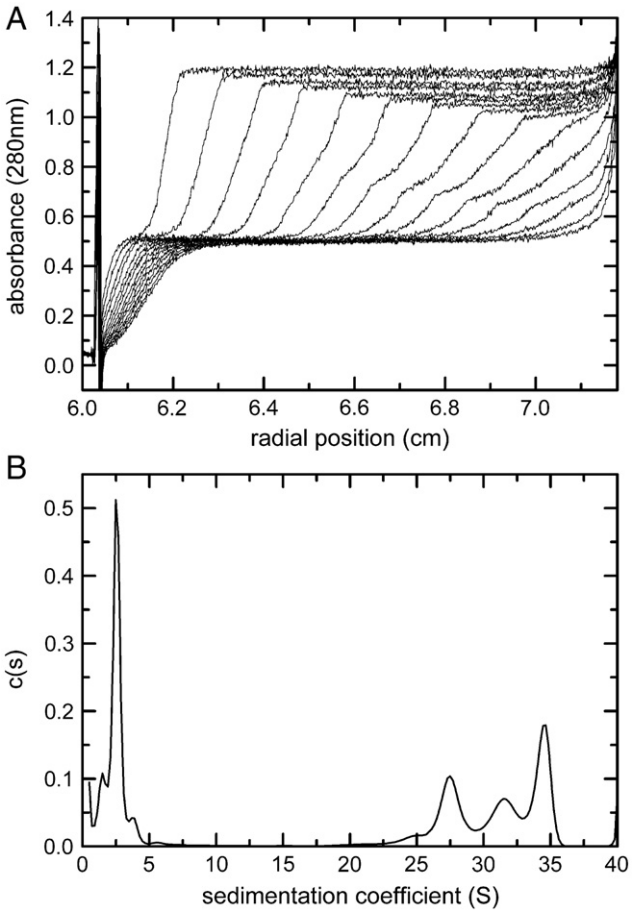

Fig. 5. Sedimentation velocity analysis of heat-treated OCP1. After heat treatment at 70 °C for 5 min, a sample of OCP1 (12.3 μM) was loaded into a dual-sector cell and sedimented at 30,000 rpm. (A) Absorbance is plotted as a function of radial position for the first fifteen scans. (B) The distribution of sedimentation coefficients obtained by analysis of the sedimentation velocity data with Sedfit.

room temperature, then subjected to sedimentation velocity analysis. The first fifteen scans from that velocity run are displayed in Fig. 5A. The distribution of sedimentation coefficients in the heat-treated sample, shown in Fig. 5B, was obtained by analyzing the entire 150-scan data set with Sedfit. Monomeric OCP1 exhibits a sedimentation coefficient of 2.3 S under these solution conditions (data not shown). Clearly, exposure to elevated temperature produces a population of rapidly sedimenting species. The appearance of peaks in the distribution at 27.5, 31.5, and 34.6 S indicates extensive aggregation. The rapidly sedimenting material constituted approximately 57% of the OCP1 in the sample. These data effectively illustrate the persistence of irreversible thermal denaturation behavior at low protein concentrations.

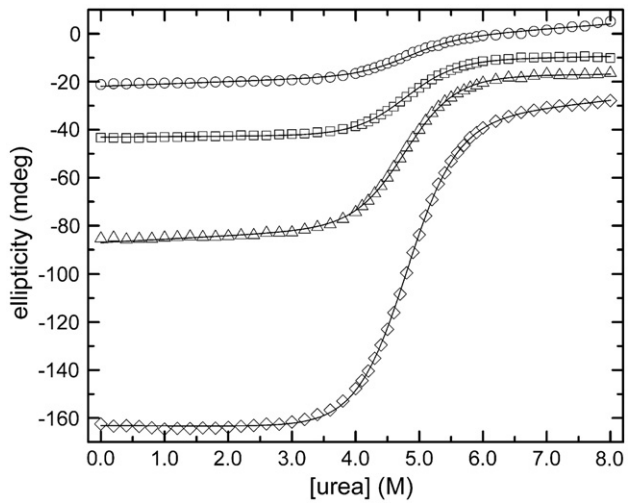

Fig. 6. Urea denaturation of OCP2. Samples of OCP2 — at concentrations of 1.2 μM (○), 2.4 μM (□), 4.8 μM (Δ), and 9.6 μM (◊), were titrated with urea, and the ellipticity of the sample was measured at 222 nm following each addition of titrant. The data, corrected for dilution, are displayed for each of the four experiments. The solid lines represent the best fit to the composite data set, employing Eqs. (1) and (2).

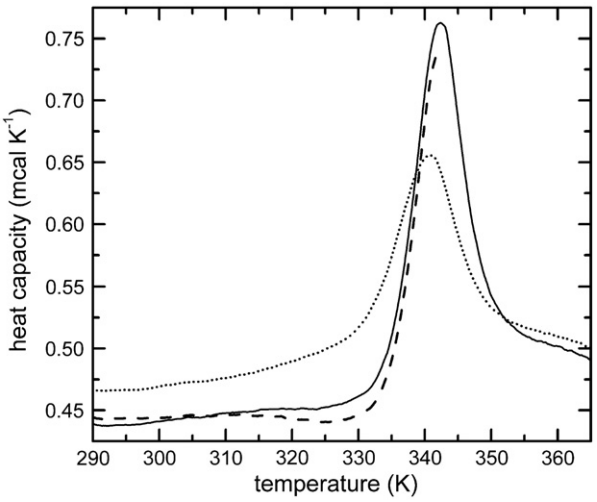

Fig. 7. Thermal denaturation of OCP2 is reversible. A sample of OCP2 (2.0 mg/mL) was heated to from 273 to 342 K in the DSC (dashed line), cooled to 273 K, then scanned from 273 to 365 K (solid line). After cooling, the sample was subjected to a second scan between 273 and 365 K (dotted line).

3.2. Characterization of OCP2/Skp1

3.2.1. Urea denaturation

OCP2 is rapidly unfolded by urea at 25 °C, in distinct contrast to OCP1. Samples of the protein — at 1.2, 2.4, 4.8, and 9.6 μM — were titrated with urea in PBS/THP (Fig. 6). Analysis of the resulting data with Eqs. (1)–(3) afforded ΔG_o and m values of 6.15 ± 0.1 kcal mol^{-1} and 1.46 ± 0.02 kcal mol^{-1} M^{-1}, respectively.

Urea-induced denaturation of OCP2 was also studied as a function of temperature between 20 and 40 °C. Those data, used in the analysis of the DSC experiments, are described below.

3.2.2. Differential scanning calorimetry

The thermal denaturation of OCP2/Skp1, monitored by DSC, is displayed in Fig. 7 (solid line). In contrast to OCP1, the denaturation of OCP2 is reversible. An endotherm is observed on rescan (dotted line), albeit reduced in amplitude and shifted to lower temperature. This behavior, often seen with reversible systems, generally results from chemical modification of the sample (e.g., oxidation, partial hydrolysis) at elevated temperatures. Lowering the high-temperature limit of the original scan improves the reproducibility. In the present case, if the first scan (dashed line) is interrupted at the transition midpoint and repeated, the amplitude of the second trace (solid line) is virtually identical to that of the truncated scan.

OCP2 was subjected to DSC analysis at concentrations of 0.95 mg/mL (51 μM monomer) and 2.15 mg/mL (116 μM monomer), and the resulting data (Fig. 8A) were treated with a two-state unfolding model (Eq. (14)). The data sets could be accommodated with a common T_m, ΔH_{cal}, and ΔH_{vH}, suggesting that there was no change in association state in the concentration range under investigation. The ratio of $\Delta H_{vH}/\Delta H_{cal}$ was 1.69.

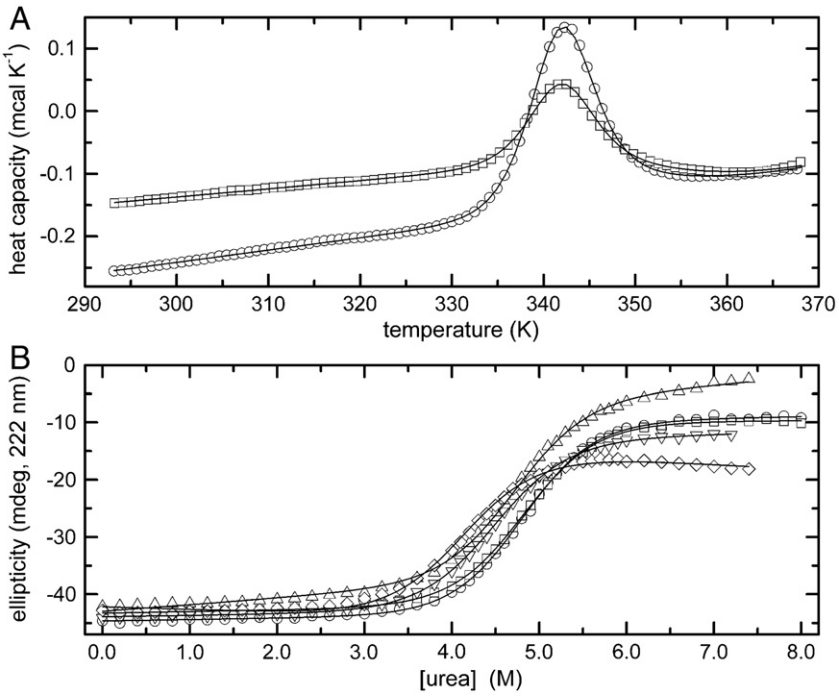

Fig. 8. Global analysis of OCP2 chemical and thermal denaturation data. (A) Analysis of OCP2, at concentrations of 50 μM (□) and 116 μM (○), were subjected to DSC analysis. The excess heat capacity is plotted as a function of the sample temperature. (B) Urea denaturation of OCP2 (2.5 μM) was performed at 20, 25, 30, 35, and 40 °C. The data, corrected for dilution, are displayed as a function of urea concentration. These data were simultaneously analyzed with the DSC data shown in panel A to obtain estimates of T_m, ΔH_{vH}, ΔH_{cal}, and ΔC_p.

To improve the estimate for ΔC_p, the DSC data were simultaneously fit with urea denaturation data collected at 20, 25, 30, 35, and 40 °C (Fig. 8B). The solid lines through the DSC and CD data denote the best weighted fit to the data. The T_m was 341.6 K; ΔH_{vH} was 102.2 kcal/mol; ΔH_{cal} was 60.4 kcal/mol; and ΔC_p was 2.10 kcal mol^{-1} K^{-1}.

3.2.3. OCP1–OCP2 complex

The OCP1–OCP2 complex was purified as described in Materials and methods. Samples of OCP1–OCP2 were subjected to urea denaturation, employing an auto-titration accessory interfaced with the CD spectrometer. The resulting data from duplicate experiments are displayed in Fig. 9A, together with the best least-squares fit to a two-state model. Because OCP1 does not unfold significantly on the timescale of this experiment, these titrations are exclusively monitoring OCP2 denaturation. The ΔG_o and m values obtained by simultaneously fitting data from two experiments to Eqs. (5) and (6) are 6.34 kcal/mol and 1.55 kcal mol^{-1} M^{-1}, respectively.

Samples of OCP1–OCP2 were also subjected to DSC, in PBS/THP. A representative denaturation profile, acquired at a scan rate of 60° h^{-1}, is displayed in Fig. 9. The thermogram is notable for the presence of two peaks. The first appears at 57.8 °C, very close to the melting temperature of OCP1 alone at the same scan rate (57.0 °C). The maximum of the second peak is positioned at 69.4 °C, likewise comparable to the T_m measured for OCP2 alone (68.4 °C). Despite the avidity with which the two proteins associate at room temperature, they evidently denature independently in the calorimeter.

3.2.4. ^1H,^{15}N-HSQC spectra of OCP1 and the OCP1/OCP2 complex

The HSQC spectra of OCP1 and OCP1–OCP2 are displayed in Fig. 10. The spectrum of OCP1 (Fig. 10A) exhibits few peaks, even when contoured at low intensity. Because OCP1 dimerizes with an apparent association constant of approximately 10^5 M^{-1} at 20 °C [10], the protein will reside in a monomer–dimer equilibrium at the concentration employed for the NMR experiment (ca. 0.3 mM). Thus, the paucity of signals may be attributable to exchange broadening resulting from the interconversion of monomeric and dimeric forms on the NMR timescale.

The spectrum of OCP1–OCP2 is likewise remarkable for the small number of peaks. The complex includes 466 main-chain amides and 32 side-chain amides. However, only a fraction of the expected signals are observed. Unlike OCP1 alone, the heterodimer exhibits no significant tendency to self-associate [10]. Thus, the appearance of the spectrum is not a consequence of interconversion between oligomeric states. Presumably, the vast majority of amide groups are sampling alternative conformations on the μs–ms timescale, with resultant signal broadening.

The OCP1 and OCP1–OCP2 spectra have been superimposed in Fig. 10C. Interestingly, a subset of the most intense signals observed in the spectrum of OCP1 alone is also present in the spectrum of the heterodimer. The implication is that a region of OCP1 remains disordered even after association with OCP2.

4. Discussion

We have previously characterized OCP1–OCP2 complex formation. At 25 °C, in Hepes-buffered saline, pH 7.4, the apparent formation constant for the complex is 4.0×10^7 M^{-1} [19]. The accompanying enthalpy change, which is not linked to protonation, is −35.9 kcal/mol. Thus, the entropic contribution is highly unfavorable ($-T\Delta S = 25.5$ kcal/mol). Association of OCP1 and OCP2 is evidently accompanied by extensive folding. In this paper, we have examined the conformational stabilities of guinea pig OCP1 and OCP2.

OCP1/Fbs1 is acidic (pI = 4.04). The 299-residue sequence from guinea pig includes 20 aspartyl- and 47 glutamyl residues. The predicted charge at pH 7.4 is −43. OCP1 is also distinguished by a high aromatic content — 12 trp and 9 tyr — as well as the presence of 16 pro and 10 cys residues. In common with all F-box proteins, the tertiary structure of the OCP1 homolog, Fbs1, includes two domains. The 110-

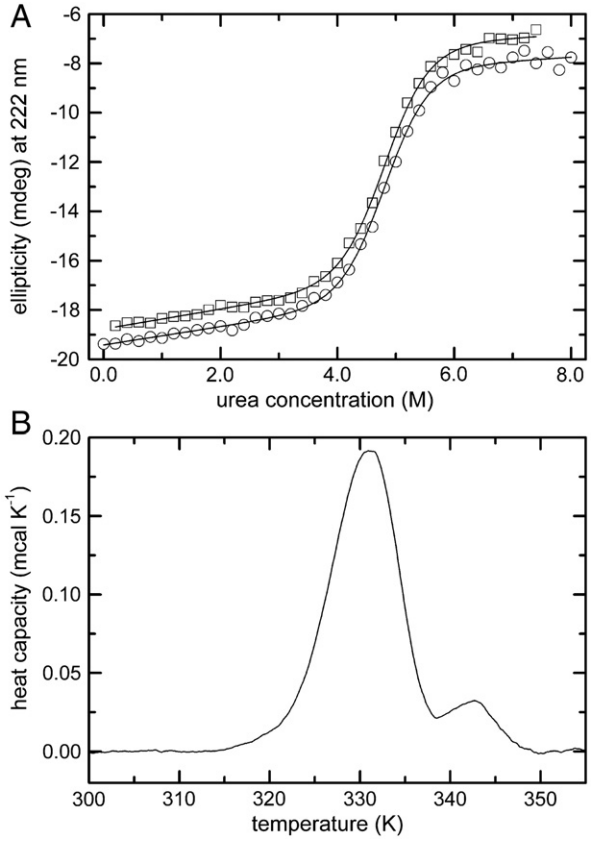

Fig. 9. Denaturation of the OCP1–OCP2 complex. (A) Samples of OCP1–OCP2 were titrated with urea at 25 °C, as described in Materials and methods. The resulting data were analyzed with a two-state unfolding model. The solid line represents the best least-squares fit. (B) A sample of the OCP–OCP2 complex (34 μM), was subjected to DSC analysis at a scan rate of 1.0° min^{-1} in PBS/THP.

residue N-terminal domain harbors the F-box motif, required for interaction with Skp1. The C-terminal domain (residues 117–297) forms the sugar-binding domain (SBD). Fbs1 is well-characterized structurally. Crystal structures are available for the SBD alone, the SBD complexed to $(GlcNAc)_2$, the SBD complexed to the glycoprotein RNase B, and the Skp1–Fbs1–chitobiose complex.

Urea-induced denaturation of OCP1 is remarkably slow, but reversible, at 25 °C. The apparent ΔG for unfolding, only 2.6 kcal/mol, suggests that the protein is marginally stable. The associated m value is likewise low, 0.79 kcal mol^{-1} K^{-1}, an indication that the change in urea-binding capacity associated with unfolding of OCP1 is unusually small.

These findings imply that OCP1 may harbor one or more disordered regions. Given the complexity of the OCP1–OCP2 association reaction, which is accompanied by the folding of roughly one hundred residues, the suggestion that OCP1 is partially disordered is quite reasonable. That hypothesis is likewise supported by analysis of the far-UV circular dichroism spectrum, which implies that a substantial percentage of the protein does not adopt regular secondary structure. It is further bolstered by the appearance of the OCP1 $^{1}H,^{15}N$-HSQC (Fig. 10). Collected in PBS/THP at pH 6.0, the spectrum is remarkable for the dearth of signals. Evidently, most of the signals undergo exchange broadening associated with monomer–dimer interconversion. The intensities and proton chemical shift values, near 8.3, for the remaining resonances are typical of amide groups that reside in "random coil" structure.

Interestingly, a substantial number of these signals persist in the OCP1–OCP2 complex. In principle, the main-chain amide groups responsible for these resonances could be located in the C-terminal domain, which is involved in target-protein binding. However, Fbs1–oligosaccharide interactions have been examined by ITC [20]. The associated entropic changes are modest, implying that Fbs1 target binding is unaccompanied by a major folding event. Alternatively, the signals could arise from residues located in the N-terminal region of OCP1. Consistent with that idea, residues 1–46 of Fbs1 are not observed in the crystal structure of the Skp1–Fbs1 complex [32], suggesting that they are disordered.

In this context, it is worth noting that the HSQC spectrum of OCP2 likewise shows some evidence of disorder [19]. OCP2, like OCP1, also forms a homodimer. However, because the association constant for dimerization is more than an order of magnitude larger, the signals arising from the ordered regions of OCP2 spectrum are not broadened away by monomer–dimer interconversion. Thus, the OCP2 spectrum is well-dispersed with the expected number of peaks.

Because thermal denaturation of OCP1 is irreversible, the data were analyzed with a two-state kinetic model [27], which assumes that the macromolecule resides in either the native or irreversibly denatured state. The N –> D conversion is governed by a rate constant k that varies with temperature in accordance with the Arrhenius rate law. The analysis yields an activation energy (E_a), a pre-exponential factor (A), and an operational calorimetric enthalpy (ΔH_{ap}). Although no systematic variation was observed for either E_a or A, the H_{cal} values trend downward from 151 to 141 to 126 kcal/mol with decreasing scan rate. Presumably, this pattern reflects greater convolution of the endothermic

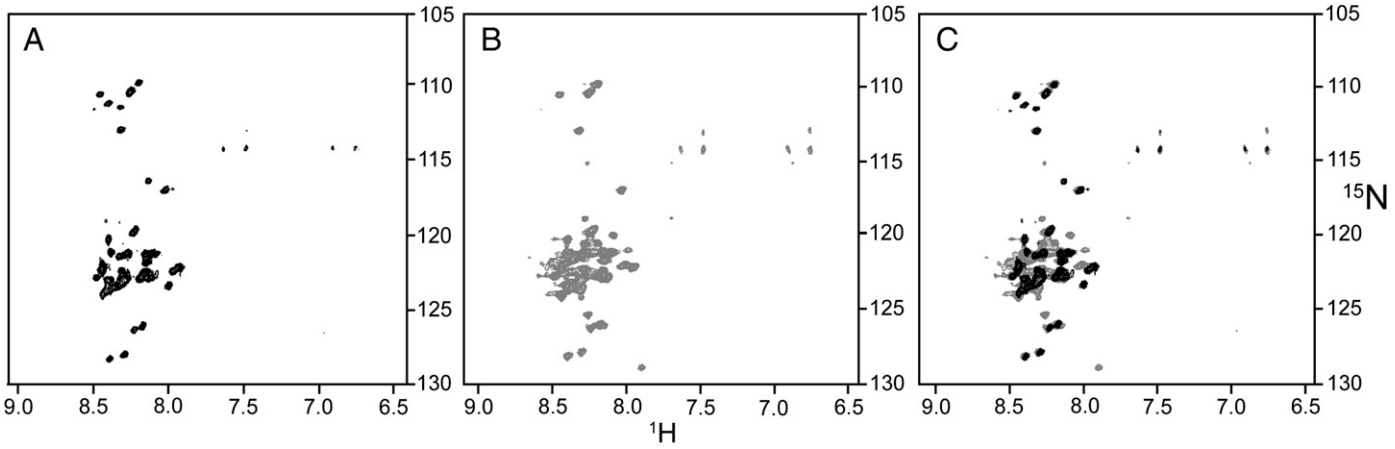

Fig. 10. TROSY-$^{1}H,^{15}$ N-HSQC spectra of OCP1 and the OCP1–OCP2 complex. (A) 0.3 mM OCP1. (B) 0.3 mM OCP1–OCP2. (C) Superposition of the OCP1 spectrum on the OCP1–OCP2 spectrum.

unfolding event and an exothermic aggregation event (vide infra) as the scan speed is reduced.

The average denaturational enthalpy value at 60 °C is roughly 7 cal g^{-1} of protein [33]. Thus, for OCP1 (M_r 34,000), one might anticipate a denaturational enthalpy on the order of 240 kcal/mol. If plotted as a function of scan speed, it appears that the apparent denaturational enthalpy would plateau well below 240 kcal/mol (Fig. 4A, inset) — additional evidence that OCP1 harbors substantial regions of disordered structure.

Although chemical modification of the polypeptide chain (e.g., hydrolysis or oxidation) can result in irreversible denaturation, it is unlikely at the relatively low temperature at which OCP1 denatures. Nonspecific aggregation is another common cause of irreversible behavior. Thermally denatured proteins frequently aggregate, due to exposure of apolar surface area. The appearance of rapidly sedimenting forms of OCP1 following heat treatment is consistent with this notion that the thermally denatured protein forms high molecular weight species.

Unlike OCP1, OCP2/Skp1 unfolds facilely in urea solutions at 25 °C. Because the protein dimerizes with an apparent association constant of 10^6 M^{-1}, the urea denaturation data, collected at OCP2 concentrations between 1.2 and 9.6 μM, were treated with a model that included the propensity for self-association. The calculations yielded a conformational free energy of 6.2 kcal/mol, and an apparent *m* value was 1.46 kcal mol^{-1} M^{-1}.

In further contrast to OCP1, thermal denaturation of OCP2 is reversible. Least-squares analysis of data acquired at two protein concentrations yielded a T_m of 69.4 °C and ΔH_{vH} and ΔH_{cal} values of 102.3 kcal/mol and 60.4 kcal/mol, respectively. The $\Delta H_{vH}/\Delta H_{cal}$ ratio is an indicator of the size of the cooperative unit. A value of 1.0 is consistent with two-state behavior, direct conversion of a (monomeric) native protein to the unfolded state. Smaller values indicate significant population of partially unfolded intermediate states. Values exceeding 1.0, on the other hand, suggest that denaturation proceeds directly from an oligomeric native state to the unfolded state. The $\Delta H_{vH}/\Delta H_{cal}$ ratio of 1.69 obtained for OCP2 implies that direct conversion of the native dimeric molecule to the unfolded state is the major pathway for unfolding.

When the DSC data were analyzed in isolation, the value of ΔC_p was not well-determined. Adapting the approach used by McCrary et al. to solve a similar problem during their characterization of Sac7d [34], we analyzed the DSC data in concert with a series of urea denaturation experiments conducted as a function of temperature, an approach suggested by Pace and Laurents [35]. Global least-squares analysis of the DSC and urea denaturation data returned a well-defined value for ΔC_p.

OCP1 and OCP2 associate tightly at 25 °C. However, because the reaction is highly exothermic, the accompanying free energy change is strongly temperature-dependent. Given the thermodynamic parameters for complex formation at 25 °C, we can use the Gibbs–Helmholtz equation to estimate the free energy change at 57 °C (the T_m for OCP1 when scanned at 1.0° min^{-1}). The value thus obtained, −5.49 kcal/mol, corresponds to an association constant of 4300 M^{-1}. If the total concentration of the OCP1–OCP2 is 50 μM, just 7.7 μM (15%) will remain associated at the elevated temperature. Consequently, when the complex is analyzed by DSC, the observed denaturation profile closely resembles the sum of the independent transitions.

5. Conclusions

OCP1 exhibits marginal stability at 25 °C, with a ΔG_{conf} value of 2.6 kcal/mol. The homodimeric OCP2 is significantly more stable, displaying a ΔG_{conf} of 6.2 kcal/mol. Whereas thermal denaturation of OCP1 is irreversible, accompanied by extensive aggregation, OCP2 denatures reversibly, with evidence that unfolding proceeds largely from the dimeric state. Although they associate avidly at 25 °C, OCP1 and OCP2 denature independently when subjected to thermal denaturation. This behavior presumably reflects the strongly exothermic nature of the interaction. The ^1H,^{15}N-HSQC spectra of OCP1 and OCP1–OCP2 are noteworthy for the striking absence of signals, presumably a consequence of exchange broadening. The relatively few peaks that remain have intensities and chemical shift values characteristic of random coil structure. The majority of signals observed in the spectrum of OCP1 alone persist in the OCP1–OCP2 complex, suggesting that one or more regions in OCP1 remain disordered upon association with OCP2.

Acknowledgment

Through a contractual agreement with Washington University in St. Louis, this work was funded in part by NIH award NIDCD/NIH 01414 (to Dr. Isolde Thalmann, Dept. of Otolaryngology).

References

[1] N.B. Slepecky, Structure of the mammalian cochlea, in: P. Dallos, A.N. Popper, R.R. Fay (Eds.), The Cochlea, Springer-Verlag, New York, 1996, pp. 44–129.
[2] S.S. Spicer, B.A. Schulte, Differences along the place-frequency map in the structure of supporting cells in the gerbil cochlea, Hear. Res. 79 (1994) 161–177.
[3] T. Kikuchi, R.S. Kimura, D.L. Paul, T. Takasaka, J.C. Adams, Gap junction systems in the mammalian cochlea, Brain Res. Rev. 32 (2000) 163–166.
[4] A. Forge, D. Becker, S. Casalotti, J. Edwards, N. Marziano, R. Nickel, Connexins and gap junctions in the inner ear, Audiol. Neurootol. 7 (2002) 141–145.
[5] F. Denoyelle, D. Weil, M.A. Maw, S.A. Wilcox, N.J. Lench, D.R. Allen-Powell, et al., Prelingual deafness: high prevalence of a 30delG mutation in the connexin 26 gene, Hum. Mol. Genet. 6 (1997) 2173–2177.
[6] D.P. Kelsell, J. Dunlop, H.P. Stevens, N.J. Lench, J.N. Liang, G. Parry, et al., Connexin 26 mutations in hereditary non-syndromic sensorineural deafness, Nature 387 (1997) 80–83.
[7] M. Cohen-Salmon, T. Ott, V. Michel, J.P. Hardelin, I. Perfettini, M. Eybalin, et al., Targeted ablation of connexin 26 in the inner ear epithelial gap junction network causes hearing impairment and cell death, Curr. Biol. 12 (2002) 1106–1111.
[8] I. Thalmann, H.L. Rosenthal, B.W. Moore, R. Thalmann, Organ of Corti specific polypeptides: OCP-I and OCP-II, Otorhinolaryngol. 226 (1980) 123–128.
[9] M.T. Henzl, J. O'Neal, R. Killick, I. Thalmann, R. Thalmann, OCP1, an F-box protein, co-localizes with OCP2/SKP1 in the cochlear epithelial gap junction region, Hear. Res. 157 (2001) 100–111.
[10] M.T. Henzl, I. Thalmann, J.D. Larson, E.G. Ignatova, R. Thalmann, The cochlear F-box protein OCP1 associates with OCP2 and connexin 26, Hear. Res. 191 (2004) 101–109.
[11] R.F. Nelson, K.A. Glenn, Y. Zhang, H. Wen, T. Knutson, C.M. Gouvion, et al., Selective cochlear degeneration in mice lacking the F-box protein, Fbx2, a glycoprotein-specific ubiquitin ligase subunit, J. Neurosci. 27 (2007) 5163–5171.
[12] P.K. Jackson, A.G. Eldridge, E. Freed, L. Furstenthal, J.Y. Hsu, B.K. Kaiser, J.D.R. Reimann, The lore of the RINGs: substrate recognition and catalysis by ubiquitin ligases, Trends Cell Biol. 10 (2000) 429–439.
[13] R. Dashaies, SCF and cullin/ring H2-based ubiquitin ligases, Annu. Rev. Cell. Dev. Biol. 15 (1999) 435–467.
[14] D. Skowyra, K.L. Craig, M. Tyers, S.J. Elledge, J.W. Harper, F-box proteins are receptors that recruit phosphorylated substrates to the SCF ubiquitin–ligase complex, Cell 91 (1997) 209–219.
[15] J.T. Winston, D.M. Koepp, C. Zhu, S.J. Elledge, J.W. Harper, A family of mammalian F-box proteins, Curr. Biol. 9 (1999) 1180–1182.
[16] Y. Liang, H. Chen, J.H. Asher, C.C. Chang, T.B. Friedman, Human inner ear OCP2 cDNA maps to 5q22–5q35.2 with related sequences on chromosomes 4p16.2–4p14, 5p13–5q22, 7pter–q22, 10 and 12p13–12qter, Gene 184 (1997) 163–167.
[17] Y. Yoshida, T. Chiba, F. Tokunaga, H. Kawasaki, K. Iwai, T. Suzuki, et al., E3 ubiquitin ligase that recognizes sugar chains, Nature 418 (2002) 438–442.
[18] J.A. Erhardt, W. Hynicka, A. DiBenedetto, N. Shen, N. Stone, H. Paulson, R.N. Pittman, A novel F box protein, NFB42, is highly enriched in neurons and induces growth arrest, J. Biol. Chem. 273 (1998) 35222–35227.
[19] A. Tan, J.J. Tanner, M.T. Henzl, Energetics of OCP1–OCP2 complex formation, Biophys. Chem. 134 (2008) 64–71.
[20] S. Hagihara, K. Totani, I. Matsuo, Y. Ito, Thermodynamic analysis of interactions between N-linked sugar chains and F-box protein Fbs1, J. Med. Chem. 48 (2005) 3126–3129.
[21] R. Thalmann, M.T. Henzl, R. Killick, E.G. Ignatova, I. Thalmann, Toward an understanding of cochlear homeostasis: the impact of location and the role of OCP1 and OCP2, Acta Otolaryngol. 123 (2003) 203–208.
[22] J.M. Galan, A. Wiederkehr, J.H. Seol, R. Haguenauer-Tsapis, R.J. Deshaies, H. Riezman, M. Peter, Skp1p and the F-box protein Rcy1p form a non-SCF complex involved in recycling of the SNARE Snc1p in yeast, Mol. Cell Biol. 21 (2001) 3105–3117.
[23] Y. Yoshida, A. Murakami, K. Iwai, K. Tanaka, A neural-specific F-box protein Fbs1 functions as a chaperone suppressing glycoprotein aggregation, J. Biol. Chem. 282 (2007) 7137–7144.
[24] N. Sreerama, R.W. Woody, Estimation of protein secondary structure from CD spectra: comparison of CONTIN, SELCON, and CDSSTR methods with an expanded reference set, Anal. Biochem. 282 (2000) 252–260.

[25] M.M. Santoro, D.W. Bolen, Unfolding free energy changes determined by the linear extrapolation method. 1. Unfolding of phenylmethanesulfonyl alpha-chymotrypsin using different denaturants, Biochemistry 27 (1988) 8063–8068.
[26] J.M. Sanchez-Ruiz, J.L. Lopez-Lacomba, M. Cortijo, P.L. Mateo, Differential scanning calorimetry of the irreversible thermal denaturation of thermolysin, Biochemistry 27 (1988) 1648–1652.
[27] E. Freire, W.W. Van Osdol, O.L. Mayorga, J.M. Sanchez-Ruiz, Calorimetrically determined dynamics of complex unfolding transitions in proteins, Annu. Rev. Biophys. Biophys. Chem. 19 (1990) 159–188.
[28] S.A. Leharne, B.Z. Chowdhry, Thermodynamic background to differential scanning calorimetry, in: J.E. Ladbury, B.Z. Chowdhry (Eds.), Biocalorimetry: Applications of Calorimetry in the Biological Sciences, Wiley, New York, 1998, pp. 157–182.
[29] P. Schuck, M.A. Perugini, N.R. Gonzales, G.J. Howlett, D. Schubert, Size-distribution analysis of proteins by analytical ultracentrifugation: strategies and application to model systems, Biophys. J. 82 (2002) 1096–1111.
[30] F. Delaglio, S. Grzesiek, G.W. Vuister, G. Zhu, J. Pfeifer, A. Bax, NMRPipe: a multidimensional spectral processing system based on UNIX pipes, J. Biomol. NMR 6 (1995) 277–293.
[31] T.D. Goddard, D.G. Kneller, Sparky vol. 3, 2007.
[32] T. Mizushima, Y. Yoshida, T. Kumanomidou, Y. Hasegawa, A. Suzuki, T. Yamane, K. Tanaka, Structural basis for the selection of glycosylated substrates by SCF^{FBs1} ubiquitin ligase, Proc. Natl. Acad. Sci. U. S. A. 104 (2007) 5777–5781.
[33] P.L. Privalov, Stability of proteins: small globular proteins, Adv. Protein Chem. 33 (1979) 167–241.
[34] B.S. McCrary, S.P. Edmondson, J.W. Shriver, Hyperthermophile protein folding thermodynamics: differential scanning calorimetry and chemical denaturation of Sac7d, J. Mol. Biol. 264 (1996) 784–805.
[35] C.N. Pace, D.V. Laurents, A new method for determining the heat capacity change for protein folding, Biochemistry 28 (1989) 2520–2525.
[36] W.L. DeLano, The PyMOL Molecular Graphics System, 2002.